University of Zurich[UZH]

Zurich Open Repository and Archive
University of Zurich
University Library
Strickhofstrasse 39
CH-8057 Zurich
www.zora.uzh.ch

Year: 2023

Structurally Simple Osmium(II) Polypyridyl Complexes as Photosensitizers for Photodynamic Therapy in the Near Infrared**

Mani, Asma ; Feng, Tao ; Gandioso, Albert ; Vinck, Robin ; Notaro, Anna ; Gourdon, Lisa ; Burckel, Pierre ; Saubaméa, Bruno ; Blacque, Olivier ; Cariou, Kevin ; Belgaied, Jamel-Eddine ; Chao, Hui ; Gasser, Gilles

DOI: https://doi.org/10.1002/anie.202218347

Posted at the Zurich Open Repository and Archive, University of Zurich
ZORA URL: https://doi.org/10.5167/uzh-253224
Journal Article
Published Version

The following work is licensed under a Creative Commons: Attribution-NonCommercial-NoDerivatives 4.0 International (CC BY-NC-ND 4.0) License.

Originally published at:
Mani, Asma; Feng, Tao; Gandioso, Albert; Vinck, Robin; Notaro, Anna; Gourdon, Lisa; Burckel, Pierre; Saubaméa, Bruno; Blacque, Olivier; Cariou, Kevin; Belgaied, Jamel-Eddine; Chao, Hui; Gasser, Gilles (2023). Structurally Simple Osmium(II) Polypyridyl Complexes as Photosensitizers for Photodynamic Therapy in the Near Infrared**. Angewandte Chemie Internationale Edition, 62(20):e202218347.
DOI: https://doi.org/10.1002/anie.202218347

Medicinal Inorganic Chemistry

How to cite: *Angew. Chem. Int. Ed.* **2023,** *62,* e202218347
International Edition: doi.org/10.1002/anie.202218347
German Edition: doi.org/10.1002/ange.202218347

Structurally Simple Osmium(II) Polypyridyl Complexes as Photosensitizers for Photodynamic Therapy in the Near Infrared**

Asma Mani[+], Tao Feng[+], Albert Gandioso[+], Robin Vinck[+], Anna Notaro, Lisa Gourdon, Pierre Burckel, Bruno Saubaméa, Olivier Blacque, Kevin Cariou, Jamel-Eddine Belgaied, Hui Chao, and Gilles Gasser**

In memory of Dr. Franz Heinemann (1989–2022)

Abstract: Five osmium(II) polypyridyl complexes of the general formula [Os(4,7-diphenyl-1,10-phenanthroline)$_2$**L**]$^{2+}$ were synthesized as photosensitizers for photodynamic therapy by varying the nature of the ligand **L**. Thanks to the pronounced π-extended structure of the ligands and the heavy atom effect provided by the osmium center, these complexes exhibit a high absorption in the near-infrared (NIR) region (up to 740 nm), unlike related ruthenium complexes. This led to a promising phototoxicity in vitro against cancer cells cultured as 2D cell layers but also in multicellular tumor spheroids upon irradiation at 740 nm. The complex [Os(4,7-diphenyl-1,10-phenanthroline)$_2$(2,2′-bipyridine)]$^{2+}$ was found to be the most efficient against various cancer cell lines, with high phototoxicity indexes. Experiments on CT26 tumor-bearing BALB/c mice also indicate that the Os^{II} complexes could significantly reduce tumor growth following 740 nm laser irradiation. The high phototoxicity in the biological window of this structurally simple complex makes it a promising photosensitizer for cancer treatment.

Introduction

Cancer is a multifactorial global issue, assumed to be the second leading cause of death in the world. According to the World Health Organization, it was responsible for 9.6 million deaths in 2018.[1] Different treatments, including radiotherapy and chemotherapy, can be used to treat this disease, quite often in combination with surgery.[2,3] However, these adjuvant treatments usually lead to severe side effects due to their lack of selectivity for diseased tissues. For this reason, many studies were conducted to develop more efficient and selective alternative treatments, as evidenced by the fact that over 60 % of all current experimental trials worldwide are focusing on cancer treatment.[3]

Photodynamic therapy (PDT) was discovered as a promising alternative/complementary technique to treat several types of cancer as well as infectious and skin diseases.[4] It relies on the simultaneous action of a photo-

[*] A. Mani,[+] A. Gandioso,[+] R. Vinck,[+] A. Notaro, L. Gourdon, K. Cariou, G. Gasser
Chimie ParisTech, PSL University, CNRS, Institute of Chemistry for Life and Health Sciences, Laboratory for Inorganic Chemical Biology
75005 Paris (France)
E-mail: gilles.gasser@chimeparistech.psl.eu
Homepage: www.gassergroup.com

A. Mani,[+] J.-E. Belgaied
National Institute of Applied Sciences and Technology, Carthage University, EcoChimie Laboratory
Tunis (Tunisia)

T. Feng,[+] H. Chao
MOE Key Laboratory of Bioinorganic and Synthetic Chemistry, School of Chemistry, Sun Yat-Sen University
Guangzhou, 510006 (P. R. China)
E-mail: ceschh@mail.sysu.edu.cn

T. Feng,[+] H. Chao
MOE Key Laboratory of Theoretical Organic Chemistry and Functional Molecule, School of Chemistry and Chemical Engineering, Hunan University of Science and Technology
Xiangtan, 400201 (P. R. China)

P. Burckel
Université de Paris, Institut de physique du globe de Paris, CNRS
75005 Paris (France)

B. Saubaméa
Cellular and Molecular Imaging Platform, US 25 Inserm, UMS 3612 CNRS, Faculté de Pharmacie de Paris, Université Paris Cité
75006 Paris (France)

O. Blacque
Department of Chemistry, University of Zurich
Winterthurerstrasse 190, 8057 Zurich (Switzerland)

[+] These authors contributed equally to this work.

[**] A previous version of this manuscript has been deposited on a preprint server (https://doi.org/10.26434/chemrxiv-2022-8gxvj).

© 2023 The Authors. Angewandte Chemie International Edition published by Wiley-VCH GmbH. This is an open access article under the terms of the Creative Commons Attribution Non-Commercial NoDerivs License, which permits use and distribution in any medium, provided the original work is properly cited, the use is non-commercial and no modifications or adaptations are made.

 © 2023 The Authors. Angewandte Chemie International Edition published by Wiley-VCH GmbH

sensitizer (PS), light and oxygen. Once administrated to the patient, the PS accumulated in the target tissues is exposed to light at a specific wavelength. The PS then reaches a relatively unstable excited singlet state, followed by an intersystem crossing from the PS singlet state to its longer-lived triplet state.[4–7] From the excited triplet state, the chromophore can then decay to the ground state by a vibronic radiation-less relaxation, producing phosphorescence, or interact with the biological environment by two different mechanisms referred to as type I or type II. In a type I mechanism, the exchange of a proton or electron occurs between the triplet excited state of the PS and the surrounding molecular oxygen to generate reactive oxygen species (ROS), such as the superoxide anion radical ($O_2^{\bullet-}$), the hydroxyl radical and other free radicals. These ROS are powerful oxidant agents capable of causing oxidative damage and hence cellular death. Alternatively, the type II mechanism is favored in oxygenated environments where the PS as a triplet state transfers its energy to ground-state molecular oxygen ($^3O_2$) to produce singlet oxygen ($^1O_2$), known for its high reactivity leading to the formation of adducts with organic substrates.[6] With its low lifetime ($\tau < 3$ µs), singlet oxygen exhibits a low intracellular diffusion distance estimated to be in the range of $2–4 \times 10^{-6}$ $cm^2 s^{-1}$ leading to a low distance of action ($\approx$0.01–0.155 µm).[7],[8] The characteristics of $^1O_2$ impart PDT with a localized effect, making it a highly selective cancer treatment.

Porphyrin-based compounds were the first developed and the most investigated PSs. However, these first-generation PSs are often insoluble in water, have poor light absorption and induce prolonged skin photosensitivity following treatment.[7] To tackle these problems, in addition to a second generation of organic PSs, metal-based PSs were developed, using different metals such as Ru^{II}, Pt^{II}, Pt^{IV}, Os^{II}, Re^{I} or Ir^{III}. Among these, Ru^{II} remains undoubtedly the most studied metal in PDT, especially Ru^{II} polypyridyl complexes, thanks to their tunable photophysical and biological properties.[9–13] Ru^{II} polypyridyl complexes have also emerged as promising agents in Photo-Activated Chemo-Therapy (PACT) thanks to their photolabile properties.[12,14] Many Ru-based PSs were evaluated in our group and others, especially coordinated with substituted 1,10-phenanthroline and 2,2'-bipyridine ligands, unveiling compounds with promising photodynamic properties.[4,9,15–18] Ru^{II} based complexes using 4,7-diphenyl-1,10-phenanthroline (DIP) ligand were efficient as PDT agents upon irradiation at 595 nm.[19] To ensure optimal light penetration in the tissues to treat deep-seated or large tumors, the excitation wavelength of the PS should ideally lie in the range of 630–850 nm. Ru^{II} complexes involving a tris-heteroleptic scaffold were used as immunoprotective photosensitizers upon irradiation at 733 nm.[20] In contrast, using two-photon instead of one-photon irradiation enables the excitation of the complexes with less energetic radiations, and thus at higher wavelengths. As such, different polypyridyl complexes based on Ru^{II} or Ir^{II} as well as bimetallic Ru^{II}-Pt^{II} complexes were shown to be photoactive in the NIR region, upon two-photon irradiation at up to 830 nm.[21]

The promising results obtained with ruthenium led us to focus on other transition metals to further improve their PDT potential. In this endeavor, osmium was shown to be the metal of choice to design new polypyridyl complexes with activation wavelengths in the NIR region.[2]

Osmium-based complexes have been proposed as DNA-binding agents in diagnostic probes for oncology. Some osmium polypyridyl complexes containing a dppz (dipyridophenazine) ligand have shown a high luminescence response at 750 nm when bound to DNA-quadruplexes.[22] Due to their spectacular luminescent properties, osmium-based complexes were applied to cancer treatment. Wang et al. have reported new dinuclear polypyridyl osmium complexes for photothermal therapy using a bridging ligand pppp ([1,10]phenanthrolino[5'',6'':5',6']pyrazino[2',3':5,6]-pyrazino [2,3-f][1,10]phenanthroline). The complex $[(Os(DIP))_2pppp]^{4+}$ revealed a high photothermal activity upon irradiation at 808 nm toward human melanoma cells.[23] McFarland et al. have also reported osmium-based PSs with exceptional photophysical properties. These complexes revealed high phototoxicity toward cancer cells upon irradiation at 730 nm.[24] However, this remarkable PDT activity is limited by the sophisticated structure of the oligothiophene-derivatized phenanthroline ligand used to prepare these complexes. In addition, no proof of in vivo efficacy was established for these complexes.[24] Lazic et al. have also developed an osmium-based PS called TLD 1829 containing the auxiliary π-extended 2,2'-biquinoline (biq) ligand. This PS demonstrated high in vivo activity against murine colon cancer after irradiation at 808 nm.[2]

The selection of complexes bearing ligands with a simpler structure, such as the DIP, is therefore of high interest. We have thus decided to develop new osmium-based PSs, with the potential to be irradiated in the NIR, enabling potentially a higher penetration depth during PDT treatments. In this work, we present the synthesis and characterization of five new osmium (II) polypyridyl complexes **1**–**5** (Figure 1). These complexes were generated from a common osmium precursor complex bearing two DIP ligands, coordinated to different bipyridine or phenanthroline derivatives: 2,2'-bipyridine (**bpy**), 4,4'-dimethyl 2,2'-bipyridine (**dmbpy**), 4,4'-diamine-2,2'-bipyridine (**dnbpy**), 1,10-phenanthroline (**phen**). The homoleptic complex **5** was obtained by coordination of the precursor with a third DIP ligand. The PDT potential of the newly synthesized complexes was then evaluated in vitro against various cancer cell lines: cervical cancer cells A2780, human and mouse colon cancer cells (HT29 and CT26). The cellular uptake and phototoxicity on 3D multicellular tumor spheroids (MCTS) were also investigated in CT-26 cells. Encouraged by promising in vitro results, we investigated the efficacy of the most promising complex (**1**) in a CT26 tumor-bearing mouse model. Our findings suggest that, with their simple structure, these new complexes have the potential to become clinically efficient one-photon NIR PDT PSs.

© 2023 The Authors. Angewandte Chemie International Edition published by Wiley-VCH GmbH

15213773, 2023, 20, Downloaded from https://onlinelibrary.wiley.com/doi/10.1002/anie.202218347 by Universitätsbibliothek Zuerich, Wiley Online Library on [19/01/2024]. See the Terms and Conditions (https://onlinelibrary.wiley.com/terms-and-conditions) on Wiley Online Library for rules of use; OA articles are governed by the applicable Creative Commons License

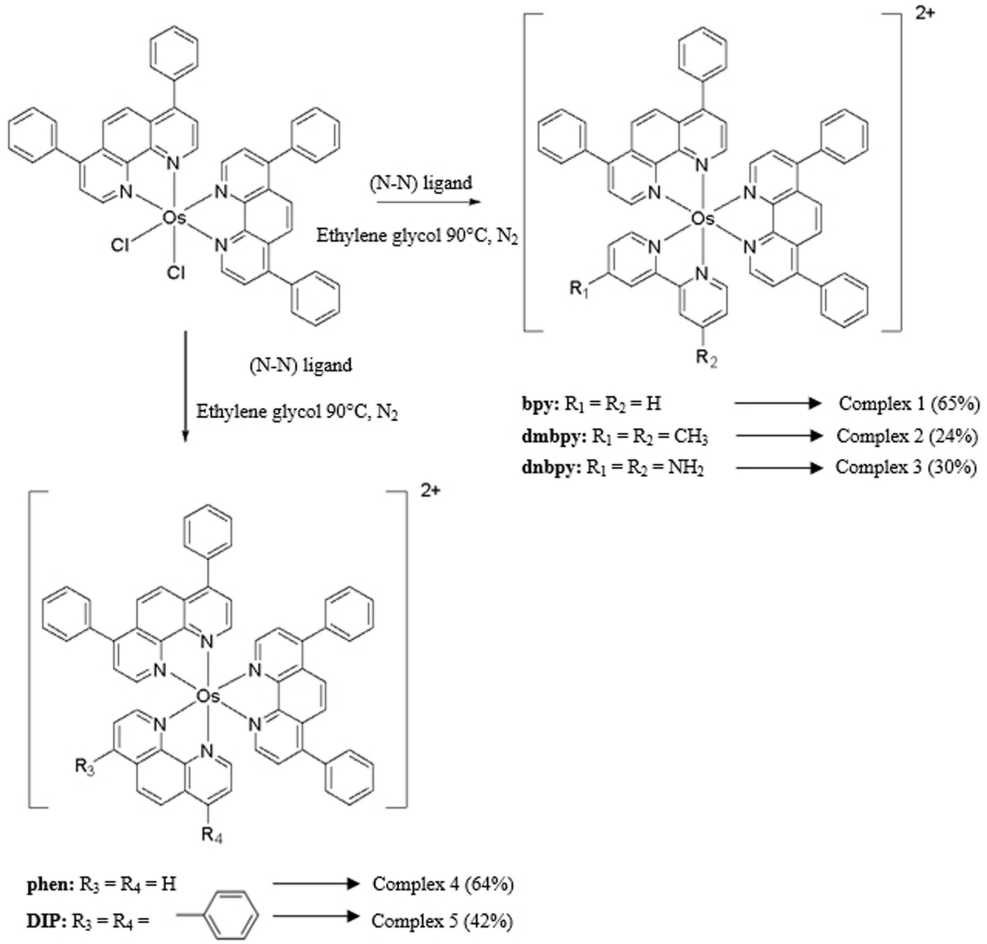

Figure 1. General synthesis route for the osmium complexes **1**–**5**.

Results and Discussion

Synthesis and characterization

The synthesis of the dichloride osmium complex $Os(DIP)_2Cl_2$ has already been reported in previous works, without detailed characterization.[25,26] However, preventing the formation of the byproduct $[Os(DIP)_3]^{2+}$ [27] while repeating the described procedure appeared challenging. After several purification attempts by silica gel chromatography, the precursor complex was successfully isolated from byproducts by precipitation from acetone in an ethanol/acetone mixture (50:1) (v/v). All the ligands were commercially available except **dnbpy**, which was synthesized as previously reported.[28] The final compounds were obtained by heating the precursor complex at 90 °C with the corresponding ligand in degassed ethylene glycol. Detailed procedures and characterizations are provided in the Supporting Information. The structure of all complexes was confirmed by ^{1}H and ^{13}C NMR spectroscopy (Figure S1–S12) and high-resolution mass spectrometry and their purity was evaluated by elemental analysis and HPLC (Figure S13). Complexes **4** and **5** were successfully crystallized by slow diffusion of diethyl ether in acetone or acetonitrile (CH_3CN), respectively. Single crystal X-ray diffraction studies were carried out.[29] Crystal data, structure refinement parameters and molecular structures are provided in the Supporting Information as well as in Figure 2 and Figure 3. For complex **4**, the Os atom is coordinated to two bathophenanthroline ligands and one substituted phenanthroline ligand through the N atoms in a distorted octahedral geometry. For complex **5**, the Os is coordinated to three bathophenanthroline ligands through the N atoms in a distorted octahedral geometry.

Photophysical properties

The UV/Visible spectrum of the different polypyridyl complexes was recorded to investigate their electronic behavior in the desired phototherapeutic window (i.e. 600–850 nm).[30] We note that the baseline for the precursor is not ideal potentially due to the formation of nanoparticles. The absorption spectrum of complexes **1**–**5** shows a panchromatic absorption from 240 to 840 nm, Figure 4. All five complexes show a similar profile, suggesting that the accessible electronic transitions, and the ground and excited states between the compounds are qualitatively similar.

© 2023 The Authors. Angewandte Chemie International Edition published by Wiley-VCH GmbH

15213773, 2023, 20, Downloaded from https://onlinelibrary.wiley.com/doi/10.1002/anie.202218347 by Universitätsbibliothek Zuerich, Wiley Online Library on [19/01/2024]. See the Terms and Conditions (https://onlinelibrary.wiley.com/terms-and-conditions) on Wiley Online Library for rules of use; OA articles are governed by the applicable Creative Commons License

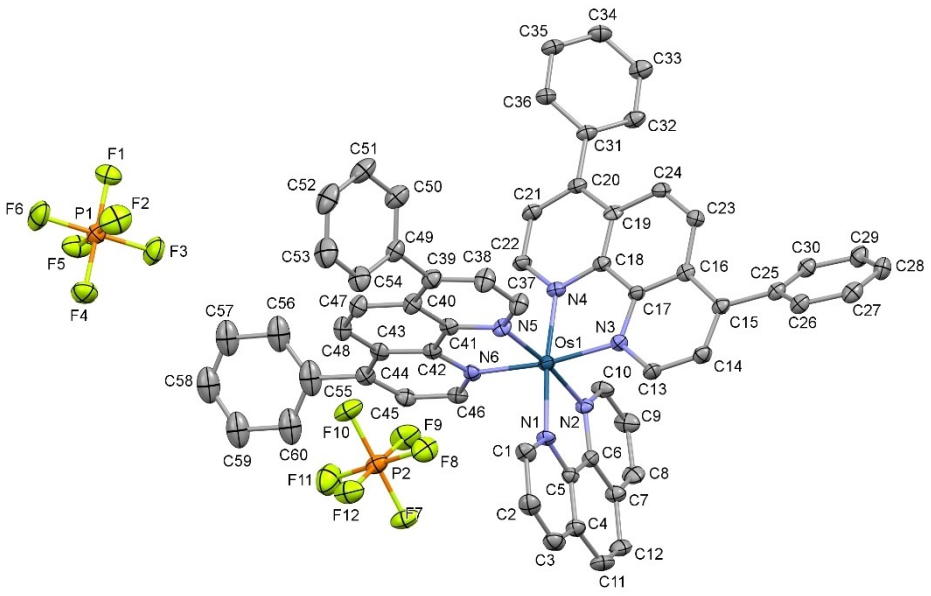

Figure 2. X-ray molecular structure of complex **4**, with hydrogen atoms omitted.

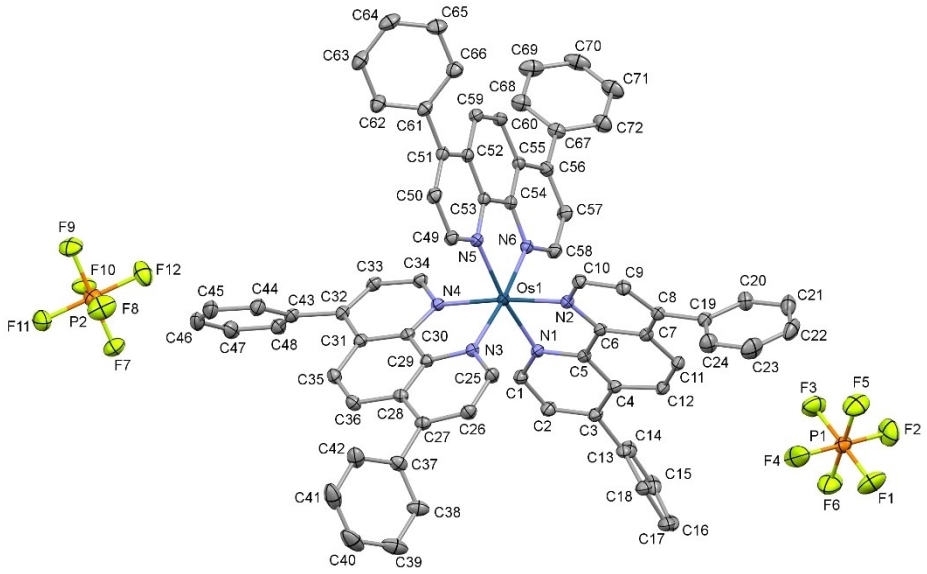

Figure 3. X-ray molecular structure of complex **5**, with hydrogen atoms omitted.

Their spectrum is however different from that of their precursor $Os(DIP)_2Cl_2$. Complexes **1**–**5** exhibit three major absorption bands, as is usually observed for related complexes. They show a sharp and intense peak at 280 nm, which can be assigned to the IL ππ* transitions of DIP, two broad peaks (with maxima at *ca.* 450 and 500 nm, respectively) attributed to the Metal to Ligand Charge Transfer (MLCT) Os(dπ)- ligand(π*), and finally a weaker broadband covering the region 650–750 nm.[25–28] This latter can be explained by the spin-forbidden MLCT transitions due to the direct singlet-triplet transition of the PS.[2,31] These transitions are explained by the strong spin-orbit coupling of osmium, often encountered in heavy atoms.[32] A similar result recently reported on $[Os(phen)_3]^{2+}$ and $[Os(DIP)_3]^{2+}$ confirms our assumptions.[24,27] Unlike their ruthenium counterparts, these complexes have therefore the potential to be phototoxic upon irradiation at wavelengths above 595 nm.[19]

Singlet oxygen ($^1O_2$) is the main toxic species for a PS working through the type II mechanism.[33,34] Therefore, the production of singlet oxygen upon irradiation of the PSs was quantitatively evaluated in CH_3CN and Phosphate Buffer Saline (PBS) using two methods.[35,36] As an indirect method, the decrease in absorbance of *p*-nitrosodimethylaniline in the presence of the photosensitizers and imidazole as $^1O_2$ scavenger was monitored as a function of the irradiation time (450 nm). The results obtained by this indirect method were confirmed by a direct method based on the quantifica-

© 2023 The Authors. Angewandte Chemie International Edition published by Wiley-VCH GmbH

15213773, 2023, 20, Downloaded from https://onlinelibrary.wiley.com/doi/10.1002/anie.202218347 by Universitätsbibliothek Zuerich, Wiley Online Library on [19/01/2024]. See the Terms and Conditions (https://onlinelibrary.wiley.com/terms-and-conditions) on Wiley Online Library for rules of use; OA articles are governed by the applicable Creative Commons License

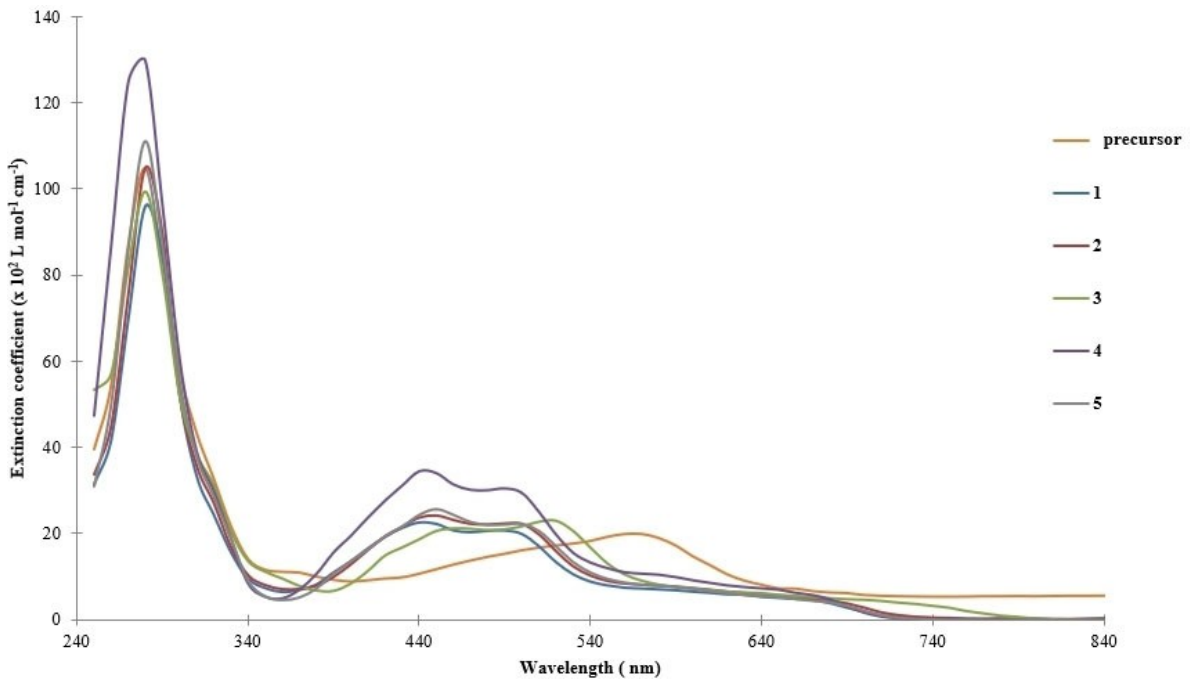

Figure 4. UV/Vis/NIR spectra of complexes **1–5** and their precursor complex in CH_3CN.

tion of the characteristic luminescence produced by the relaxation of $^1O_2$.[35,36] The singlet oxygen quantum yields were then calculated using $[Ru(bpy)_3]Cl_2$ and phenalenone as references in PBS and CH_3CN, respectively.

Both methods showed that all complexes but **3** efficiently sensitize oxygen with quantum yields of 35–50 % in aerated CH_3CN and 2.6–6.2 % in aerated PBS, Table 1. The lower yields obtained with complex **3** may be explained by the presence of a diamine group, which is able to quench the singlet oxygen, as reported previously.[37,38] The quenching mechanism is due to a charge transfer between the ground state of a nitrogen-containing compound and singlet oxygen.[38] The quantum yield in aqueous media appeared lower than in CH_3CN. The low singlet oxygen production in aqueous media can be related to the strong quenching properties of water.[39] Unfortunately, the singlet oxygen production yield could not be determined in deuterated water D_2O using the direct method as the luminescence signal was under the detection limit.

Despite low $^1O_2$ production yields in polar aqueous media, our compounds could still prove to be efficient PSs since cells include apolar environments. Indeed, it was previously demonstrated that, upon interaction with hydrophobic components of the cell such as DNA, PSs that otherwise produce a low level of $^1O_2$ in water can efficiently sensitize molecular oxygen.[40]

(Photo-)toxicity

To evaluate the (photo-)cytotoxic effect of the synthesized complexes, a screening was performed on cervical cancer cells (A2780) and non-cancerous retinal pigment epithelial (RPE-1) cells. For this purpose, cells were incubated with 0.1, 1, or 10 μM of compounds **1–5** in the dark for 4 hours. After washing, they were then either kept in the dark or irradiated for 1 h at 620 nm (spectral half-width: 32 nm, 60 min, 1.88 mW cm^{-2}, 6.7 J cm^{-2}), 645 nm (spectral half-width: 32 nm, 60 min, 2.50 mW cm^{-2}, 9.0 J cm^{-2}), 670 nm

Table 1: **1–5** singlet oxygen quantum yields ($\Phi(^1O_2)$) in CH_3CN and aqueous solutions determined by direct and indirect methods upon excitation at 450 nm.

Compound	CH_3CN	CH_3CN	D_2O	PBS
	Direct method [%]	Indirect method [%]	Direct method [%]	Indirect method [%]
1	35	39.7	n.d	6.2
2	37	41.5	n.d	4.3
3	9	20.7	n.d	1.7
4	40	39.9	n.d	5.9
5	50	43.4	n.d	2.6

n.d. = not determinable.

© 2023 The Authors. Angewandte Chemie International Edition published by Wiley-VCH GmbH

15213773, 2023, 20, Downloaded from https://onlinelibrary.wiley.com/doi/10.1002/anie.202218347 by Universitätsbibliothek Zuerich, Wiley Online Library on [19/01/2024]. See the Terms and Conditions (https://onlinelibrary.wiley.com/terms-and-conditions) on Wiley Online Library for rules of use; OA articles are governed by the applicable Creative Commons License

(spectral half-width: 32 nm, 60 min, 3.75 mW cm^{-2}, 13.5 J cm^{-2}), 740 nm (spectral half-width: 32 nm, 60 min, 3.50 mW cm^{-2}, 12.6 J cm^{-2}). The cell viability was determined 2 days later using a fluorometric assay. For comparative purposes, the clinically approved PDT photosensitizer Protoporphyrin IX (PpIX) was included in this study.

This first screening showed that compounds **1**–**5** have no cytotoxic effect at up to >10 μM in the dark in A2780 and RPE-1 cells (Figure S20). In contrast, all compounds induced high phototoxicity upon light exposure at all tested wavelengths in the two cell lines (Figure S21). While complexes **1**, **3** and **4** led to a potent reduction of cell viability at concentrations as low as 1 μM, complexes **2** and **5** only revealed their phototoxic effect at 10 μM. Of note, no significant selectivity towards cancer cells was observed in this preliminary assay. Importantly, we could demonstrate that complexes **1**–**4** were able to have a phototoxic effect at up to 740 nm. In light of these promising results, the phototoxicity of the complexes was evaluated in more detail. Because of their structural similarity with **1** (for **2**) and their relatively poor phototoxicity (for **5**), both complexes **2** and **5** were excluded from further investigations. The concentration of complexes **1**, **3**, and **4** needed to kill 50 % of the cells (IC_{50}) was determined following 4 hours of incubation and 1 hour of irradiation at 740 nm or 4 hours of incubation in the dark in A2780 and RPE-1 cells, Table 2. All complexes appeared less toxic than PpIX in the dark ($IC_{50}=3\pm2$ μM), with **1** and **3** exhibiting the lowest cytotoxicity ($IC_{50}=58\pm9$ μM and 62 ± 10 μM, respectively). With the exception of PpIX, the IC_{50} of every compound significantly decreased upon light irradiation at 740 nm, confirming their potential as PDT PSs. Of note, **1** displayed the highest phototoxicity index (PI = 118), defined as the ratio between dark toxicity and phototoxicity, against A2780 cells. Similar results were obtained on healthy RPE-1 cells, confirming the absence of selectivity towards cancer cells.

Since complex **1**, as a PF_6 salt, was revealed to be the most efficient PS at 740 nm, and in view of future in vivo experiments in a colon tumor mouse model, an additional phototoxicity evaluation was performed on human and mouse colon adenocarcinoma (HT29 and CT26) cells. For this purpose, the PF_6^- counter ion was exchanged by chloride ions Cl^-, using an Amberlite IRA-410, to ensure better solubility in biological fluids, mainly later for in vivo tests. The results presented in Table 2 show that complex **1** displays similar and high phototoxicity in the two cell lines ($IC_{50}=0.33\pm0.03$ μM and 0.34 ± 0.06 μM for HT29 and CT26, respectively). Of note, the same phototoxicity was observed with the structurally similar ruthenium complex $[Ru(DIP)_2dmbpy]^{2+}$ in CT26 cells upon irradiation at 540 nm using the same low light dose (14.2 J cm^{-2}) ($IC_{50}=0.34\pm0.005$ μM).[19] In contrast, the phototoxicity of the osmium complex $[Os(DIP)_2(dpp)]^{2+}$, where dpp = 2,3-bis(2-pyridyl)pyrazine, was previously tested in the rat glioma cells F98, following irradiation at 625 nm and showed a significantly lower anticancer activity ($IC_{50}=86.1\pm8.5$ μM) than that our complex **1**.[41]

The dinuclear osmium complexes $[(Os(DIP))_2pppp]^{4+}$, described previously, demonstrated a high photothermal activity toward human melanoma cells, using higher complex concentrations (≥10 μM) upon irradiation at 808 nm.[23] Furthermore, complex **1** with a Cl^- counterion was found to be cytotoxic after irradiation with near-infrared light in the micromolar range in hypoxic conditions (IC_{50}, 740 nm = 4.75 ± 0.30 μM, IC_{50}, dark = 46.44 ± 1.0 μM, PI = 10) (Figure S23–S25). Importantly, we could demonstrate that complex **1** exhibits a phototoxic effect at up to 740 nm, even under hypoxic conditions, an important requirement for a PDT agent.

The impressive results obtained with complex **1** against the three tested cell lines A2780, CT-26, and HT29 at 740 nm, a NIR wavelength, prompted us to submit it to additional experiments before initiating in vivo studies.

Table 2: IC_{50} values in normoxic and hypoxic conditions, in the dark and upon irradiation at 740 nm (spectral half-width: 32 nm, 60 min, 3.50 mW cm^{-2}, 12.6 J cm^{-2}) for **1**, **3**, and **4** compared to **PpIX** on non-cancerous retinal pigment epithelium (RPE-1), cervical cancer (A2780) cells, human colon cancer (HT29) cells and mouse colon adenocarcinoma (CT-26) cells. Average of three independent measurements.

Normoxic conditions		Dark	740 nm (1 h, 12.6 J cm^{-2})	PI
PpIX	A2780	3 ± 2 μM	2.2 ± 0.2 μM	2
	RPE-1	4 ± 2 μM	6 ± 2 μM	n.d
1	A2780	58 ± 9 μM	0.49 ± 0.09 μM	118
	RPE-1	47 ± 2 μM	0.54 ± 0.03 μM	87
3	A2780	62 ± 10 μM	1.3 ± 0.3 μM	48
	RPE-1	76 ± 9 μM	2.9 ± 0.6 μM	27
4	A2780	19 ± 2 μM	0.51 ± 0.07 μM	37
	RPE-1	26.7 ± 0.5 μM	0.77 ± 0.06 μM	35
1*	HT29	14 ± 1 μM	0.33 ± 0.03 μM	42
	CT26	13.1 ± 0.3 μM	0.34 ± 0.06 μM	39
Hypoxic conditions		**Dark**	**740 nm (1 h, 12.6 J cm^{-2})**	**PI**
PpIX	CT-26	>100 μM	35.5 ± 0.6 μM	>2.8
1[a]	CT-26	46 ± 1.0 μM	4.8 ± 0.3 μM	10

n.d. = not determinable. [a] The counter ion was exchanged from PF_6^- to chloride Cl^-.

© 2023 The Authors. Angewandte Chemie International Edition published by Wiley-VCH GmbH

15213773, 2023, 20, Downloaded from https://onlinelibrary.wiley.com/doi/10.1002/anie.202218347 by Universitätsbibliothek Zuerich, Wiley Online Library on [19/01/2024]. See the Terms and Conditions (https://onlinelibrary.wiley.com/terms-and-conditions) on Wiley Online Library for rules of use; OA articles are governed by the applicable Creative Commons License

Photostability

An important parameter to assess is the (photo-)stability of a PS. For this reason, the stability of **1**–**5** was evaluated. The stability was first determined in the dark by observing changes in the UV/Vis spectrum of the complexes over 48 hours of incubation in different media. This experiment suggests that all complexes are stable in CH_3CN, PBS, and DMSO (Figure S15–S17). Of note, complexes were found to be poorly soluble in PBS, requiring supplementation with 1% DMSO. Since PDT requires light application, the photocytotoxicity activity of photosensitizer candidates is strongly influenced by their photostability upon irradiation. For this reason, we performed photo-stability studies of complexes **1**–**5** at 37 °C in biologically relevant media (i.e. PBS and DMEM medium (Gibco) supplemented with 10% FBS) (Figure S18 and S19) upon irradiation at 740 nm for 1 h. No significant changes in the absorption spectra of complexes **1**–**5** were observed in PBS and DMEM after 1 h of irradiation.

Cellular uptake and localization studies

The cellular uptake of our osmium complexes **1**–**5** was then investigated in CT-26 cells by determining the amount of Os inside the cells using inductively coupled plasma mass spectrometry (ICP-MS) after 4 h of incubation at 10 μM, (Figure 5). The Os complex $[Os(DIP)_3](PF_6)_2$ (**5**) was found to have the highest uptake, almost three times higher than the rest of the complexes. This is probably due to the higher lipophilicity of the DIP ligand compared to bpy and phen. The uptake of **1** and **2** is also 2-fold higher in comparison to complexes **3** and **4**. The lower uptake of complexes **3** and **4** might be due to the lower solubility of these complexes. The incorporation of NH_2 into the bpy (complex **3**) decreases the internalization of the complex. Unfortunately, we could not establish a relationship between the accumulation and their photo-toxicity values because all the complexes described herein present a similar photo-toxicity.

To get further insight into the internalization mechanism of complex **1**, its subcellular localization was determined by confocal microscopy using the intrinsic luminescence of our Os^{II} complex (λ_{ex} = 448 nm, λ_{em} = 645–730 nm). In CT26 cells incubated with 5 μM complex **1** for 4 hours, the luminescence appeared as both a diffuse and a punctate signal suggesting the accumulation of the complex in both the cytosol and some vesicular compartments (Figure 5). However, the complex did not accumulate in the nucleus and mitochondria as shown by the absence of colocalization with Hoechst 33342 and MitoTracker Green respectively.

Phototoxicity on 3D multicellular tumor spheroids (MCTS)

Complex **1** was found to be the most promising candidate among the series of osmium complexes investigated in a 2D cell model. Due to its remarkably high and promising photocytotoxicity, we explored its activity in a multicellular tumor spheroid (MCTS) model. In 3D spheroids, MCTS simulates the conditions in clinically treated tumors, including an hypoxic environment, and the extracellular matrix deposition. Additionally, the growth pattern, metabolism, and gene expression mimic the complexity of the initial stages of solid tumors. These features allow for a reasonable estimation of in vivo antitumor activity, qualifying MCTS as a more reliable model than monolayer cell cultures for advanced cancer research.[42,43]0.

An experiment was therefore performed to evaluate the time-dependent effect on the growth of MCTSs treated with

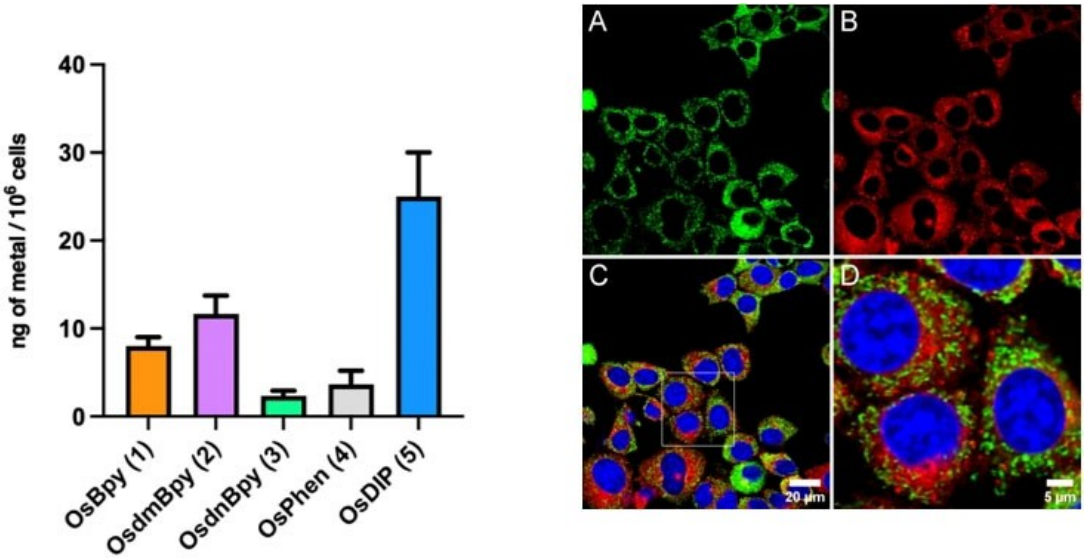

Figure 5. (Left) Cellular uptake of compounds **1**–**5** by ICP-MS (Right) Cellular uptake of complex **1** by confocal microscopy. A) Mitochondria-specific dye MitoTracker Green (green, exc: 488 nm, em: 513–550 nm) B) Complex **1** (red, exc: 448 nm, em: 645–730 nm) C) Overlay plus nucleus-specific dye Hoechst 33342 (blue, exc: 405 nm, em: 409–448 nm) D) Higher magnification of the boxed area in (C).

© 2023 The Authors. Angewandte Chemie International Edition published by Wiley-VCH GmbH

15213773, 2023, 20, Downloaded from https://onlinelibrary.wiley.com/doi/10.1002/anie.202218347 by Universitätsbibliothek Zuerich, Wiley Online Library on [19/01/2024]. See the Terms and Conditions (https://onlinelibrary.wiley.com/terms-and-conditions) on Wiley Online Library for rules of use; OA articles are governed by the applicable Creative Commons License

complex **1**. CT26 MCTSs (ca. 550 μm in diameter) were treated with increasing concentrations of **1** (0,1, 1, 10, 30, and 100 μM). After 36 h of incubation, a luminescence signal is observed in the spheroids (Figure S22). The medium was then exchanged with fresh medium, and cells were kept in the dark or irradiated for 1 h at 740 nm. Following this treatment, half of the medium in the wells was exchanged every two days, and pictures of the spheroids were taken (Figure 6). Importantly, CT26 MCTSs treated with the highest concentrations of 30 μM and 100 μM of complex **1** had a reduced diameter. In contrast, no effect was seen in MCTSs treated with the complex and kept in the dark (100 μM) in comparison to untreated MCTS. In addition, complex **1** was tested via a luminescent cell viability assay in CT-26 MCTS (single graphs are available in Figure S23). Complex **1** displayed high cytotoxicity toward CT-26 MCTSs with $IC_{50} \approx 31 \pm 6$ μM. This result is comparable to the IC_{50} obtained with $[Ru(DIP)_2dmbpy]^{2+}$ in HeLa MCTS.[19]

Overall, the outstanding activities shown by complex **1** in the monolayer cell model were confirmed in an MCTS model. This is of high interest since the center of spheroids is considered hypoxic (i.e., with a low concentration of oxygen) and it could be anticipated that our complex would be efficient in further experiments *in vivo* These findings are a powerful motivation for further investigation of complex **1** as a novel potential photosensitizer agent in photodynamic therapy.

Dynamic Light Scattering (DLS)

We previously observed that Ru^{II} complexes incorporating two DIP ligands could form aggregates in isotonic aqueous solutions.[44] While they form large aggregates in PBS, we recently showed that they can form smaller nanoparticles in the presence of plasmatic proteins. As it is the case with positively charged gold nanoparticles, we postulated that the presence of salt decreases the repulsive electrostatic interaction between the Ru^{II} complexes, resulting in their aggregation.[45] This aggregation was prevented in culture medium by the coating effect provided by plasmatic proteins, leading to the formation of sub-micron nanoparticles.[46] As this aggregation behavior could affect the biodistribution of the complexes in vivo, we performed a Dynamic Light Scattering (DLS) analysis to investigate the aggregation behaviour of complex **1** with a Cl^- counterion in 10 % FBS in PBS. The DLS analysis of 10 % FBS in PBS without the complex revealed the existence of nanometric objects with a mean diameter of 8.87 nm, which could correspond to serum albumin.[47] In the presence of complex **1** with a Cl^- counterion, a subtle shift in the mean diameter of the objects from 8.87 to 12.68 could be observed (Figure S14). This small shift could be explained by the binding of the complex to albumin, as observed previously with other drugs.[48] In 100 % PBS, complex **1** with the Cl^- counterion tends to form larger particles that sediment, which can be observed with the naked eye and is confirmed by the high polydispersity index obtained by DLS. Therefore, in contrast to our previously described Ru^{II} complexes, for which nanoparticles of up to 350 nm were observed in the presence of plasmatic proteins, complex **1** appears to be soluble in this medium, probably thanks to its binding to plasmatic proteins.

In Vivo Studies

Encouraged by the promising results obtained in vitro with complex **1** in 2D and 3D models, its PDT efficacy was further investigated in a CT26 tumor-bearing BALB/c mouse model. One hour following intratumoral injection, the mice were either kept in the dark or exposed to one-photon irradiation using a 740 nm laser (50 mW, 12.6 J cm^{-2}, 300 s). The tumor volume and body weight of each mouse

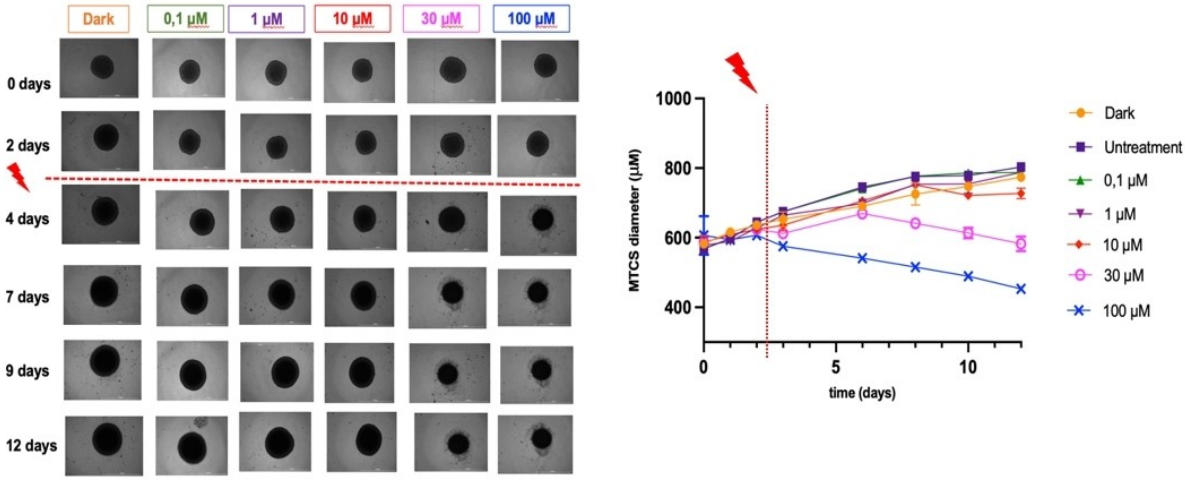

Figure 6. (Left) Changes in the growth kinetics of MCTSs treated with complex **1** at different concentrations (0,1, 1, 10, 30, and 100 μM). Images were collected on days 0, 2, 4, 7, 9, and 12. (Right) MCTS diameter was measured at different time points. Average of three independent measurements.

© 2023 The Authors. Angewandte Chemie International Edition published by Wiley-VCH GmbH

15213773, 2023, 20, Downloaded from https://onlinelibrary.wiley.com/doi/10.1002/anie.202218347 by Universitätsbibliothek Zuerich, Wiley Online Library on [19/01/2024]. See the Terms and Conditions (https://onlinelibrary.wiley.com/terms-and-conditions) on Wiley Online Library for rules of use; OA articles are governed by the applicable Creative Commons License

was measured and recorded every two days for two weeks. According to the tumor growth inhibition curve (Figure 7A), the tumors treated with complex **1** and light were found to be nearly eradicated within a single procedure. On day 14, the normalized tumor volume in the complex **1**+Light group was 4.67, 4.56 and 4.36-fold smaller than the control group, the group treated with light only and the group treated with complex **1** without irradiation, respectively (Figure 7A, C and D). Importantly, the animals treated with complex **1** behaved normally, without signs of pain, stress or discomfort and did not lose weight, suggestive of the high biocompatibility of the compound (Figure 7B). After the treatment, all major organs (i.e., heart, liver, spleen, lung, kidney, brain, intestine) as well as the tumor tissues were histologically examined by the hematoxylin-eosin stain. While no pathological alterations or injuries were observed for all organs (Figure S24), significant damages including karyopyknosis and widespread areas of apoptotic nuclei were noticed in the tumor tissue (Figure 7E). Terminal deoxynucleotidyl transferase dUTP nick end labeling (TUNEL) stain was employed to analyze tumor tissues. The green fluorescence signals, indicative of DNA strand breaks during apoptosis, for the treatment with complex **1**+Light were observed, indicative of the strong therapeutic effect. As discussed in the introduction, the Os-based complex TLD 1829 showed high survival in murine population bearing colon cancer as well, after irradiation at 808 nm (600 J cm^{-2}, 4 h).[2] TLD 1829 and complex **1** showed comparable in vivo activity with the advantage of a lower light exposure of complex **1** (740 nm, 12.6 J cm^{-2}, 1 h) compared to TLD1829 (808 nm, 600 J cm^{-2}, 4 h). Overall, this study demonstrates the important potential of complex **1** for photodynamic therapy in the biological window.

Conclusion

In summary, we were able to prepare and characterize structurally simple Os^{II} polypyridyl complexes bearing two bathophenanthroline ligands. These complexes showed excellent photophysical properties, including high $^1O_2$ production quantum yields. Importantly, they displayed a panchromatic absorption which enables the irradiation of the PS at wavelengths up to 740 nm. This wavelength is much higher in comparison to the maximum wavelength at which the ruthenium analog $[Ru(DIP)_2dmbpy]^{2+}$ can be excited. Cell experiments on all complexes in non-cancerous retinal pigment epithelium (RPE-1) and cervical cancer cells A2780 showed no cytotoxicity in the dark and intense toxicity following light irradiation. Importantly, complex **1**, with its simple structure, was found to have a promising PI value at 740 nm with low dark toxicity and an IC_{50} in the nanomolar range following irradiation. It also proved to be extremely stable and highly phototoxic against human and mouse colon cancer cells (HT29 and CT26). The high $^1O_2$ production quantum yield and absorption properties of complex **1** endow it with an excellent PDT efficacy in vivo. Such simple Os^{II} polypyridyl complexes may indeed become promising antitumor therapeutic agents for future clinical applications.

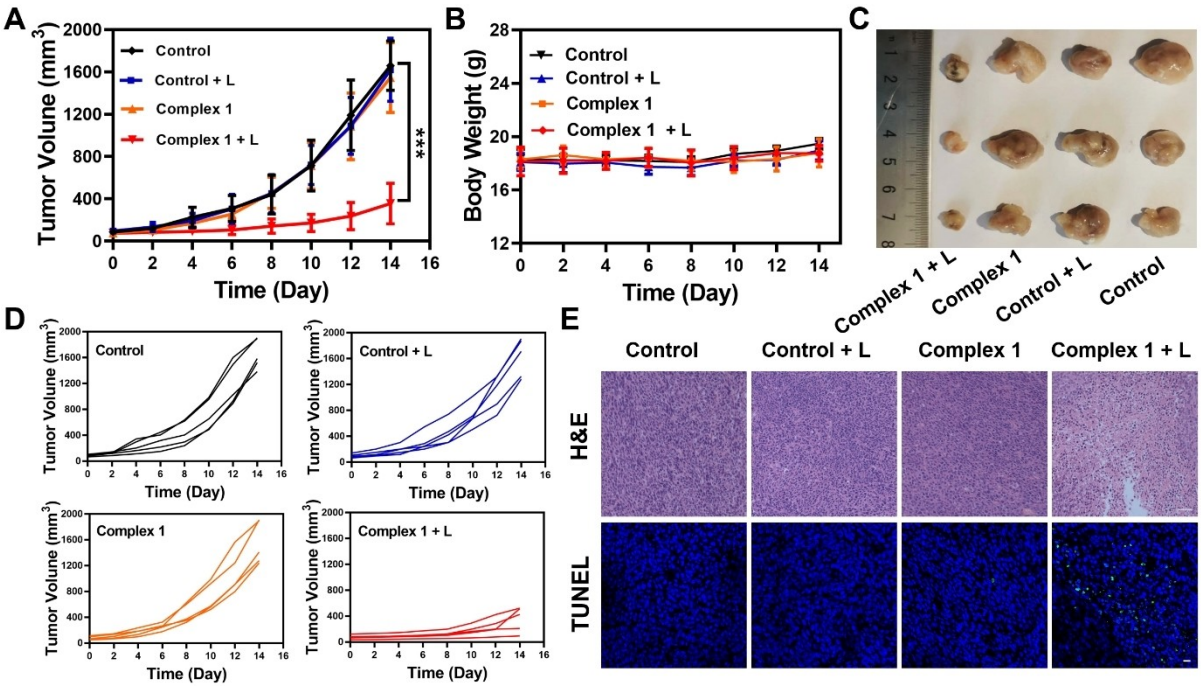

Figure 7. A) Average tumor growth curves after the respective treatment ($n=5$) Dose: 5.0 mg kg^{-1}; Irradiation (740 nm; 50 mW, 12.6 J cm^{-2}, 300 s). B) Time-dependent change in body weight after various treatments on mice. C) Representative pictures of the tumor after the respective treatments. D) Individual tumor growth curves after the respective treatments. E) Haematoxylin-eosin (H&E) stain (scale bar: 200 μm) and TUNEL stain (scale bar: 100 μm) of the tumor tissues after the respective treatments. *** $P<0.001$. Average of five independent measurements.

© 2023 The Authors. Angewandte Chemie International Edition published by Wiley-VCH GmbH

15213773, 2023, 20, Downloaded from https://onlinelibrary.wiley.com/doi/10.1002/anie.202218347 by Universitätsbibliothek Zuerich, Wiley Online Library on [19/01/2024]. See the Terms and Conditions (https://onlinelibrary.wiley.com/terms-and-conditions) on Wiley Online Library for rules of use; OA articles are governed by the applicable Creative Commons License

Supporting Information

^{1}H and ^{13}C NMR spectra (Figure S1–S12). HPLC traces (Figure S13). Size distribution by volume (Figure S14). Absorption spectra for stability evaluation in the dark (Figure S15–S17). Absorption spectra for photobleaching evaluation (Figure S18 and S19). Viability tests (Figure S20 and S21). Fluorescence microscopy of CT-26 spheroids treated with complex **1** (Figure S22). Fluorometric cell viability assay in normoxic conditions in CT26 MCTS after irradiation at 740 nm (Figure S23). Fluorometric cell viability assay in hypoxia conditions in CT26 MCTS after irradiation at 740 nm (Figure S24 and S25). Hypoxia chamber (Figure S26). Histological examination of all major organs by a hematoxylin-eosin stain (Figure S27).

Acknowledgements

This work was financially supported by an ERC Consolidator Grant Photo-MedMet to G.G. (GA 681679), has received support under the program "Investissements d'Avenir" launched by the French Government and implemented by the ANR with the reference ANR-10-IDEX-0001-02 PSL (G.G.) and by a Qlife pré-maturation funding (G.G. and R.V.). A.G. thanks the ARC Foundation for cancer research for a postdoctoral Research Fellowship. Part of the ICP-MS measurements was supported by IPGP multidisciplinary program PARI, and by Paris-IdF region SESAME Grant no. 12015908. The authors thank Mathilde Chaboud and Dr. Philippe Goldner for their help in the determination of singlet oxygen quantum yield as well as Dr. Gregory Lefevre for lending the DLS apparatus. This work was also supported by the National Natural Science Foundation of China (No. 22120102002), and the Science and Technology Innovation Program of Hunan Province of China (No. 2021RC5028). L.G. acknowledges the ENS-PSL for her PhD fellowship.

Conflict of Interest

The authors declare no competing financial interests.

Data Availability Statement

The data that support the findings of this study are available from the corresponding author upon reasonable request.

Keywords: Bioinorganic Chemistry · Infrared · Medicinal Inorganic Chemistry · Osmium · Photodynamic Therapy

[1] World Health Organisation, "Cancer." https://www.who.int/news-room/fact-sheets/detail/cancer (accessed Mar. 05, 2022).
[2] S. Lazic, P. Kaspler, G. Shi, S. Monro, T. Sainuddin, S. Forward, K. Kasimova, R. Hennigar, A. Mandel, S. McFarland, L. Lilge, *Photochem. Photobiol.* **2017**, *93*, 1248–1258.
[3] Z. Abbas, S. Rehman, *Neoplasma* **2018**, 139–157.
[4] F. Heinemann, J. Karges, G. Gasser, *Acc. Chem. Res.* **2017**, *50*, 2727–2736.
[5] C. Marie, V. Pierroz, S. Ferrari, G. Gasser, *Chem. Sci.* **2015**, *6*, 2660–2686.
[6] I. Macdonald, T. Dougherty, *J. Porphyrins Phthalocyanines* **2001**, *5*, 105–109.
[7] A. O'Connor, W. Gallagher, A. Byrne, *Photochem. Photobiol.* **2009**, *85*, 1053–1074.
[8] P. Ogilby, *Chem. Soc. Rev.* **2010**, *39*, 3181–3209.
[9] S. Monro, K. Colon, H. Yin, J. Roque, P. Konda, S. Gujar, R. Thummel, L. Lilge, C. Cameron, S. McFarland, *Chem. Rev.* **2019**, *119*, 797–828.
[10] R. Caspar, C. Cordier, J. Werner, C. Guyard-Duhayon, M. Gruselle, P. Le Floch, H. Amouri, *Inorg. Chem.* **2006**, *45*, 4071–4078.
[11] B. Howerton, D. Heidary, E. Glazer, *J. Am. Chem. Soc.* **2012**, *134*, 8324–8327.
[12] L. Conti, E. Macedi, C. Giorgi, B. Valtancoli, V. Fusi, *Coord. Chem. Rev.* **2022**, *469*, 214656.
[13] L. He, Y. Li, C. Tan, R. Ye, M. Chen, J. Cao, L. Ji, Z. Mao, *Chem. Sci.* **2015**, *6*, 5409.
[14] S. Bonnet, *Dalton Trans.* **2018**, *47*, 10330–10343.
[15] S. McFarland, A. Mandel, R. Dumoulin-White, G. Gasser, *Curr. Opin. Chem. Biol.* **2020**, *56*, 23–27.
[16] L. McKenzie, H. Bryant, J. Weinstein, *Coord. Chem. Rev.* **2019**, *379*, 2–29.
[17] L. Zeng, P. Gupta, Y. Chen, E. Wang, L. Ji, H. Chao, Z. Chen, *Chem. Soc. Rev.* **2017**, *46*, 5771–5804.
[18] J. Karges, *Angew. Chem. Int. Ed.* **2022**, *61*, e202112236.
[19] J. Karges, F. Heinemann, M. Jakubaszek, F. Maschietto, C. Subecz, M. Dotou, R. Vinck, O. Blacque, M. Tharaud, B. Goud, E. Viñuelas Zahínos, B. Spingler, I. Ciofini, G. Gasser, *J. Am. Chem. Soc.* **2020**, *142*, 6578–6587.
[20] L. Lifshits, J. Roque, P. Konda, S. Monro, H. Cole, D. von Dohlen, S. Kim, G. Deep, R. Thummel, C. Cameron, S. Gujar, S. McFarland, *Chem. Sci.* **2020**, *11*, 11740–11762.
[21] J. Karges, H. Chao, G. Gasser, *J. Biol. Inorg. Chem.* **2020**, *25*, 1035–1050
[22] K. Peterková, M. Stitch, R. Boota, P. Scattergood, P. Elliot, M. Towrie, P. Podbevšek, J. Plavec, S. Guinn, *Chem. Eur. J.* **2022**, *28*, e202203250.
[23] M. Wang, Y. Deng, Q. Li, S. Tang, R. Yang, R. Zhao, F. Liu, X. Ren, D. Zhang, F. Gao, *Chem. Commun.* **2022**, *58*, 12676–12679.
[24] J. Roque, P. Barrett, H. Cole, L. Lifshits, G. Shi, S. Monro, D. von Dohlen, S. Kim, N. Russo, G. Deep, C. Cameron, M. Alberto, S. McFarland, *Chem. Sci.* **2020**, *11*, 9784–9806.
[25] B. Carlson, G. Phelan, W. Kaminsky, L. Dalton, X. Jiang, S. Liu, A. Jen, V. Uni, *J. Am. Chem. Soc.* **2002**, *124*, 14162–14172.
[26] E. Kober, J. Caspar, P. Sullivan, T. Meyer, *Inorg. Chem.* **1988**, *27*, 4587–4598.
[27] Y. Wei, M. Zheng, L. Chen, X. Zhou, S. Liu, *Dalton Trans.* **2019**, *48*, 11763–11771.
[28] O. Maury, J. Guégan, T. Renouard, A. Hilton, P. Dupau, N. Sandon, L. Toupet, H. Le Bozec, *New J. Chem.* **2001**, *25*, 1553–1566.
[29] Deposition Numbers 2175814 (for complex **4**) and 2175813 (for complex **5**) contain the supplementary crystallographic data for this paper. These data are provided free of charge by the joint Cambridge Crystallographic Data Centre and Fachinformationszentrum Karlsruhe Access Structures service.
[30] K. Plaetzer, B. Krammer, J. Berlanda, F. Berr, T. Kiesslich, *Lasers Med. Sci.* **2009**, *24*, 259–268.
[31] E. Kianfar, D. Apaydin, G. Knör, *ChemPhotoChem* **2017**, *1*, 378–382.

© 2023 The Authors. Angewandte Chemie International Edition published by Wiley-VCH GmbH

15213773, 2023, 20, Downloaded from https://onlinelibrary.wiley.com/doi/10.1002/anie.202218347 by Universitätsbibliothek Zuerich, Wiley Online Library on [19/01/2024]. See the Terms and Conditions (https://onlinelibrary.wiley.com/terms-and-conditions) on Wiley Online Library for rules of use; OA articles are governed by the applicable Creative Commons License

[32] B. Carlson, G. Phelan, J. Benedict, W. Kaminsky, L. Dalton, *Inorg. Chim. Acta* **2006**, *359*, 1093–1102.
[33] P. Maharjan, H. Bhattarai, *J. Oncol.* **2022**, *2022*, 7211485.
[34] L. Schiff, W. Eisenberg, J. Dziuba, K. Taylor, S. Moore, *Environ. Health Perspect.* **1987**, *76*, 199–203.
[35] A. Leonidova, V. Pierroz, R. Rubbiani, J. Heier, S. Ferrari, G. Gasser, *Dalton Trans.* **2014**, *43*, 4287–4294.
[36] J. Karges, F. Heinemann, F. Maschietto, M. Patra, O. Blacque, I. Ciofini, B. Spingler, G. Gasser, *Bioorg. Med. Chem.* **2019**, *27*, 2666–2675.
[37] A. Nakajima, H. Akamatu, *Bull. Chem. Soc. Jpn.* **1968**, *41*, 1961–1963.
[38] R. Young, R. Martin, D. Feriozi, D. Brewer, R. Kayser, *Photochem. Photobiol.* **1973**, *17*, 233–244.
[39] I. Belousova, O. Danilov, V. Kiselev, I. Kislyakov, T. Kris'ko, T. Murav'eva, D. Videnichev, *Laser Optics 2006: Wavefront Transformation and Laser Beam Control* **2007**, *6613*, 76–87.
[40] C. Mari, V. Pierroz, R. Rubbiani, M. Patra, J. Hess, B. Spingler, L. Oehninger, J. Schur, I. Ott, L. Salassa, S. Ferrari, G. Gasser, *Chem. Eur. J.* **2014**, *20*, 14421–14436.
[41] J. Zhu, A. Dominijanni, J. Rodriguez-Corrales, R. Prussin, Z. Zhao, T. Li, J. Roberston, K. Brewer, *Inorg. Chim. Acta* **2017**, *454*, 155–161.
[42] H. Ma, Q. Jiang, S. Han, Y. Wu, J. Tomshine, D. Wang, Y. Gan, G. Zou, X. Liang, *Mol. Imaging* **2012**, *11*, 487–498.
[43] J. Friedrich, C. Seidel, R. Ebner, L. Kunz-Schughart, *Nat. Protoc.* **2009**, *4*, 309–324.
[44] A. Notaro, G. Gasser, A. Castonguay, *ChemMedChem* **2020**, *15*, 345–348.
[45] A. Albanese, W. Chan, *ACS Nano* **2011**, *5*, 5478–5489.
[46] R. Vinck, A. Gandioso, P. Burckel, B. Saubaméa, K. Cariou, G. Gasser, *Inorg. Chem.* **2022**, *61*, 13576–13585.
[47] X. Yang, M. Bolsa-Ferruz, L. Marichal, E. Porcel, D. Salado-Leza, F. Lux, O. Tillement, J. Renault, P. Serge, F. Wien, S. Lacombe, *Int. J. Mol. Sci.* **2020**, *21*, 4673.
[48] T. Hushcha, A. Luik, Y. Naboka, *Talanta* **2000**, *53*, 29–34.

Manuscript received: January 19, 2023
Accepted manuscript online: March 14, 2023
Version of record online: April 12, 2023

© 2023 The Authors. Angewandte Chemie International Edition published by Wiley-VCH GmbH

15213773, 2023, 20, Downloaded from https://onlinelibrary.wiley.com/doi/10.1002/anie.202218347 by Universitätsbibliothek Zuerich, Wiley Online Library on [19/01/2024]. See the Terms and Conditions (https://onlinelibrary.wiley.com/terms-and-conditions) on Wiley Online Library for rules of use; OA articles are governed by the applicable Creative Commons License